UNIVERSITY OF THE
WITWATERSRAND,
JOHANNESBURG

Mechatronics Systems Design Analysis and Control

Project B : Solar tracker

Group 7

Sandile	**Nkosi**	**2117587**
Kago	**Letlhaku**	**1938942**
Hlanhla	**Hlungwane**	**1538138**
Thabo	**Dhladhla**	**2103812**

An assignment submitted to the Faculty of Engineering and the Built Environment,

University of the Witwatersrand, Johannesburg, in partial fulfilment of the requirements for

The degree of Bachelor of Science in Engineering. Johannesburg, May 2024

UNIVERSITY OF THE WITWATERSRAND, JOHANNESBURG

SCHOOL OF MECHANICAL, INDUSTRIAL & AERONAUTICAL ENGINEERING

Disclosure – Use of Artificial-Intelligence (AI) Generated Content

2024 V2

Students must acknowledge all use of AI.

Select all applicable statements and complete the sections fully. Delete all statements that are not applicable.

1. Disclosure: Editing/refining grammar, spelling, formatting

☒ I acknowledge the use of Grammarly , version 1.2.671336 , in May 2024 to improve the spelling, grammar and formatting of the document. The software was installed and added on in Microsoft word.

The output from these prompts was used as explain what the code was used for.

☒ ***I declare that the disclosure is complete and truthful.***

Student number: 2117587
Student number: 1938942
Student number: 1538138
Student number: 2103812
Course code: MECN4029A
Date: 14 May 2024

EXECUTIVE SUMMARY

In this paper, a solar tracker was to be designed that would control panels in the Sandton area. To do this the steps of dynamics investigation were followed. Firstly, the solar tracker physical elements were selected: this included the solar panels, sensors to be used on the control and the actuator that was to be used. Following this was the mathematical modelling, which was done in two parts, the first part was the use of the generic equations (Newton's laws of motion and Kirchoff's current laws), and these were then linearised using Taylor's series expansion method about the system's equilibria. The system was then analysed for stability in both the time and frequency domain and a conclusion was made that an active control system was necessary for the control of the solar tracker system. Performance specifications that would guide the control of the system were drawn and two controller design methods were investigated. This is the root locus controller design, and the Proportional, Integral, and Derivative (PID) control techniques were used. These were able to control the solar tracker to within the required specifications and were used on a simulated winter and summer day.

CONTENTS

LIST OF FIGURES

LIST OF TABLES

NOMENCLATURE

A	Area of panels (maximum taken)
b	Drag moment arm
C_m	Panels drag coefficient
C_{motor}	Motor friction coefficient
C_{panels}	Panels friction coefficient
h	Sun hour angle
J_{motor}	Motor shaft moment of inertia
J_{panels}	Panel assembly moment of inertia
K_t	Motor torque constant
L_{motor}	Motor coil inductance
L_S	Sandton latitude
r_{large} , r_{small}	Pulley radii
T_1	Motor torque
T_2	Panel torque
V_m	Maximum amplifier voltage
Z_S	Sandton altitude
α	Solar altitude angle
δ	Sun inclination angle
θ	Panel orientation
$\theta_{\max}$	Maximum amplifier read angle
ρ	Air density

1 Introduction

1.1 Solar Tracker Introduction

In response to the recent surge in power outages plaguing South Africa, a prominent company based in Sandton has decided to take proactive measures by transitioning to solar energy. Recognizing the potential of solar power to mitigate the impact of load shedding, the company is eager to invest in a robust solar panel system. These panels, comprising photovoltaic cells typically made of semiconductor materials like silicon, offer a promising solution to the energy challenges faced by the region.

To optimize energy generation, my team and I have been entrusted to select the most suitable solar panel components and design an efficient control system for solar tracking. The solar tracking system adjusts the position of solar panels to track the Sun's movement and its position during the day, maximizing Sunlight exposure throughout the day. In our pursuit of an optimal solution, we are considering the implementation of a single-axis horizontal solar tracker. This horizontal-axis solar tracker is suitable for low-latitude areas [1] and the amount of energy harvested is usually sufficient.

Sandton, nestled in the northern part of Johannesburg, South Africa, boasts a prime location with coordinates approximately 26.1076° S latitude and 28.0567° E longitude [2]. Characterized by a subtropical highland climate, the region experiences hot, wet summers and mild, dry winters, fostering an environment conducive to solar energy generation. With over 2,500 hours of Sunshine annually, Sandton basks in ample solar irradiance, making it an ideal candidate for solar panel installations [3].

Understanding the intricacies of the Sun's trajectory is pivotal in designing an efficient solar tracking control system. In Sandton, the Sun's journey from east to west unfolds predictably each day, ensuring consistent exposure to Sunlight. Moreover, the area's flat topography (1513 m) offers an unobstructed canvas for solar panel orientation, minimizing shading and maximizing solar absorption [4].

Wind patterns and wind speed play a crucial role in ensuring the structural resilience and accurate tracking of the Sun by the solar panel system. Sandton experiences moderate wind conditions, with an average wind speed of 17 km/h (4.7 m/s) [5]. Thus, engineering the system to withstand typical wind speeds is imperative for its long-term durability and stability.

By considering these factors, the team aim to craft a solar panel system with a solar tracking control system that is not only optimized for Sandton's unique climate and geographical features but also engineered to deliver reliable and sustainable energy solution.

2 Modelling

To investigate the dynamics of a system, there are specific steps that one must follow and iterate. These steps are mentioned in [6] as:

Step 1: Physical modelling

Step 2: Equations of motion (Mathematical modelling)

Step 3: Dynamic behaviour

Step 4: Design decisions

These steps are thus followed to model and thus, bring about the control of the solar tracker system to be modelled.

2.1 Physical modelling

In the development of a solar tracking control system, the selection and integration of components play a crucial role in ensuring optimal performance and efficiency. Among the key components utilized in such a system are the potentiometer, motor, pulleys, belt, and solar panels. Each component contributes uniquely to the system's functionality, enabling precise tracking of the Sun's movement to maximize energy capture.

2.1.1 Amplifier

An amplifier is an electronic device that boosts control signals from a controller to provide the necessary power for driving a motor. Since the input signal will be quite small to drive a motor, an amplify such as one depicted in Figure 2.1. will ne used for driving the motor.

Figure 2.1: Motor drive unit [7]

2.1.2 Potentiometer

A potentiometer, depicted in Figure 2.2 below serves as a crucial sensor in the solar tracking control system, providing feedback on the position of the solar panels relative to the Sun.

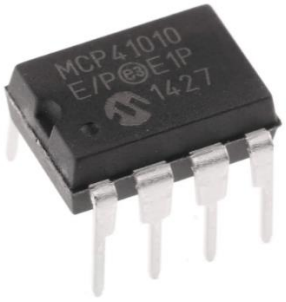

Figure 2.2: Digital potentiometer [8]

Mounted on the tracking mechanism, it detects changes in panel orientation and generates a voltage signal proportional to the angle of rotation. This feedback signal is fed into the control system, enabling real-time adjustments to ensure optimal alignment with the Sun's position throughout the day. By accurately measuring panel angles, the potentiometer enables precise tracking and maximizes energy capture.

2.1.3 Motor

At the heart of the solar tracking control system is the motor, which drives the movement of the solar panels, this is shown in Figure 2.3.

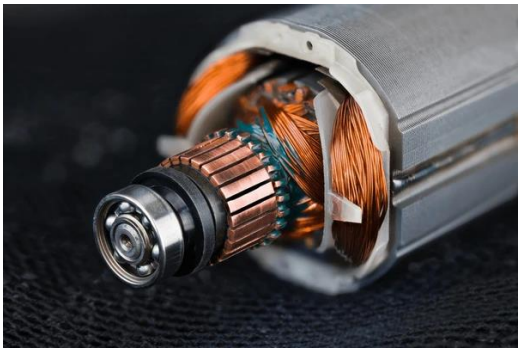

Figure 2.3: Field-controlled DC motor [9]

The motor receives control signals from the system based on feedback from the potentiometer and adjusts the panels' position accordingly. Typically connected to the tracking mechanism, the motor provides the necessary torque to overcome friction and mechanical resistance during panel movement.

By controlling the motor's speed and direction, the control system ensures smooth and accurate tracking of the Sun’s movement, optimizing energy generation.

2.1.4 Pulleys and Belt

Pulleys and belts, Figure 2.4, form an integral part of the mechanical linkage system that translates the motors’ rotational motion into linear movement to adjust the solar panels' orientation.

Figure 2.4: Pulley's and belt system [10]

The motor drives one of the pulleys, which is connected to a belt looped around multiple pulleys distributed along the solar panels' mounting structure. As the motor rotates, the belt transfers motion to the pulleys, causing the panels to tilt or rotate as needed to track the Sun using the Sun’s position throughout the day. This mechanical arrangement provides a reliable and efficient means of translating rotary motion into linear motion, enabling precise and synchronized panel tracking.

2.1.5 Solar Panels

The solar panels, Figure 2.5 below, are the primary components responsible for capturing Sunlight and converting it into electrical energy. Mounted on the tracking mechanism, they are continuously adjusted to track the Sun's movement throughout the day using the Suns’ position. By maintaining an optimal angle relative to the Sun, the panels maximize Sunlight exposure and energy capture. The control system ensures that the panels are oriented optimally, minimizing shading, and maximizing energy output. Through effective coordination with the other components, the solar panels play a crucial role in achieving efficient energy generation in the solar tracking system.

Figure 2.5: Solar panel configuration with solar panels [11]

2.2 Architecture of the solar panel model

The model architecture is represented below in Figure 2.6 below. The motor gets its power from a source through an amplifier. The motor then drives the solar panel through pulleys through the belt connection.

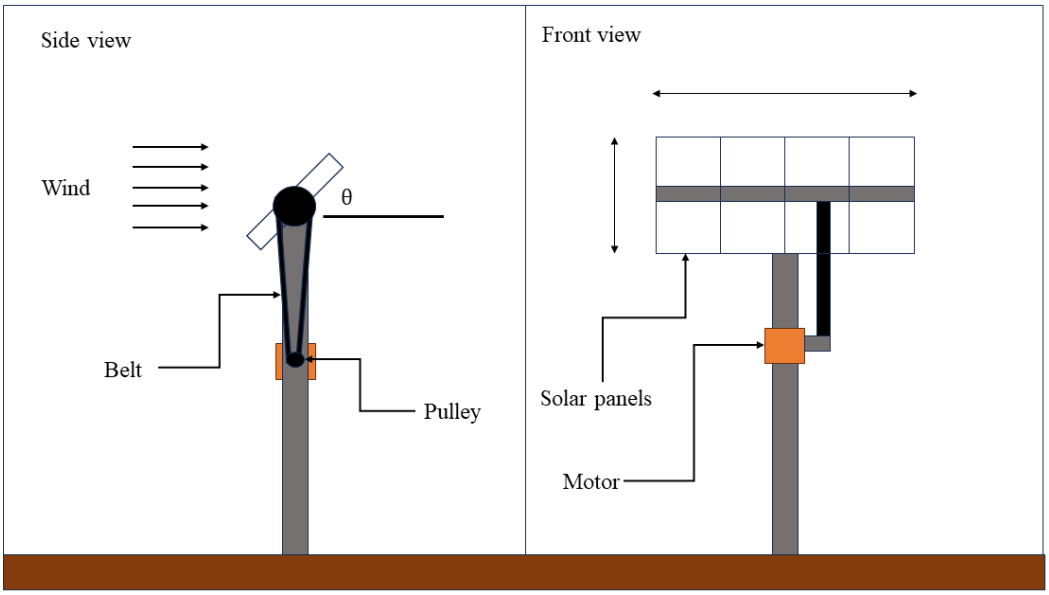

Figure 2.6: Solar panel assembly physical mode

2.3 Nonlinear physical model

2.3.1 Amplifier

The potentiometer measures the angular position of the solar panels, translating mechanical movement into electrical signals for precise tracking. The equations governing the amplifier function are summarised below:

$$V_{out} = \frac{V_{max}}{\theta_{max}} * \theta_{in} \quad (1)$$

Where V_{out} is the instant output voltage of the amplifier, V_{m} is the maximum possible output voltage of the amplifier with a constant value of 12 V, θ_{in} is the input position angle value at any instant and θ_{max} is the maximum position that the amplifier can read out with a constant value of 2**π** rad.

2.3.2 Field-Controlled DC Motor

This motor, regulated by control voltages, translates electrical input into torque, providing the necessary mechanical power to adjust the position of the solar panels. The circuit diagram of such a motor system is in Figure 2.7 below.

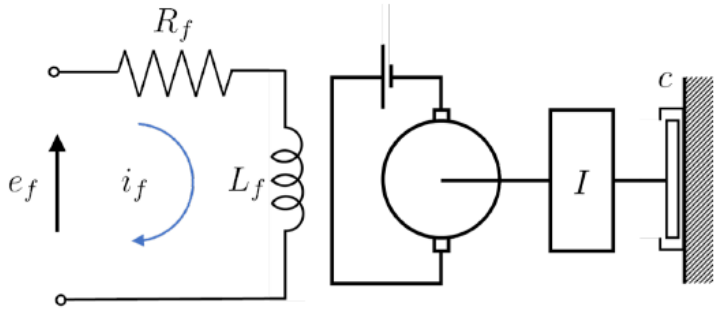

Figure 2.7: Field controlled DC motor [6]

The equations governing the torque and the output voltage are summarised below [6].

$$e_f(t) - i_f(t)R_f = L_f \frac{di_f(t)}{dt} \quad (2)$$

$$T_1 = K_t * i_f(t) \quad (3)$$

Where e_f is the field input voltage which is equal to the potentiometer output voltage at any instant, i_f is the field current passing through the components, R_f is the motor wiring resistance, L_f is the motor

wiring inductance and T_1 is the motor output torque.

2.3.3 Sprockets and belt drive

Working in tandem, the sprockets and belt drive system efficiently transmit the torque from the motor to the solar panels, amplifying it as needed for smooth and accurate positioning of the solar panels.

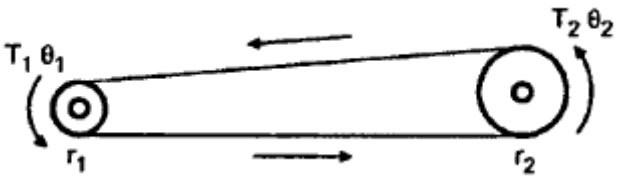

Figure 2.8: Belt connection between pulleys [12]

The belt is assumed to be a massless, linear and a non-flexible element and the equation governing the functioning of the belt connection is given by:

$$T_2 = \frac{r_2}{r_1} T_1 \tag{4}$$

Where r_1 and r_2 are the motor pulley and panel pulley radii respectively and T_2 is the torque that is driving the panels.

2.3.4 Solar Panel Array

Comprising four panels, this pivotal system maximizes Sunlight exposure by adjusting its orientation based on the torque provided by the motor. The differential equation governing the functioning of the solar panel is given by [13]:

$$T_2 - M_{wind} - M_{bearing} = M_{panels} \tag{5}$$

$$T_2 - \frac{1}{2}\rho C_m A V^2 b - c_{panels}\dot{\theta} = J_{panels}\ddot{\theta} \tag{6}$$

Where ρ is the density of the air, C_m is the panel drag coefficient, A is the panel area, V is the velocity of the wind, b is the wind moment arm of the panel, c_{panels} is the bearing coefficient of friction, J_{panels} is the panel moment of inertia and θ is the angular displacement of the panel.

Assumptions:

- $J_{panels} >> J_{motor}$ and thus J_{motor} can be regarded as negligible.
- $C_{panells} >> C_{motor}$ and this C_{motor} can be regarded as negligible
- A – the area of the panel is constant (so that the system has constant coefficients and is easier to analyse). The maximum value of A is taken for this analysis.

2.4 Linearized and the linear model

The potentiometer, motor, and gear systems in the above model are linear systems. The equation governing the solar panel configuration is however nonlinear due to the square velocity term and ought to be linearized. Linearisation is a process of representing a nonlinear equation by its linear counterpart about an equilibrium position(s). To linearise the equation above the average velocity of the chosen area, Sandton, was found to be 4.77 m/s and will thus be taken as the equilibrium position for this solar panel system and can be linearised using the Taylor series expansion [6]. We can rearrange equation (6) and let it be equal to some function f and use the Taylor series expansion.

$$f(y) \simeq f(y_0) + \frac{\partial f}{\partial y_0}(y - y_0) \tag{7}$$

$$f = T_{out} - \frac{1}{2}\rho C_m A V^2 b - c_{panels}\dot{\theta} - J_{panels}\ddot{\theta} \tag{8}$$

Thus, the linearised equation is thus given by:

$$\Delta T_{out} - \rho C_m A V_0 \Delta V b - c_{panels}\Delta\dot{\theta} = J_{panels}\Delta\ddot{\theta} \tag{9}$$

Where V_0 is the standard velocity of the wind in Sandton of about 4.77 m/s. Now with the equation governing the motion of the solar panel linearised, all the equations governing the control of the solar tracker are linear and can be represented using a transfer function. A transfer function is a mathematical representation describing the relationship between the input and output of a system. To get the transfer function, we take the Laplace transform of each of the linear equations. Equations 1, 2, 3, 4, and 9. The resulting equations after mathematical manipulation are summarized below.

$$\frac{V_{out}(s)}{\theta_{in}(s)} = \frac{V_{\max}}{\theta_{max}} \tag{10}$$

$$\frac{I(s)}{V_{out}(s)} = \frac{1}{L_{motor}\, s + R_{motor}} \tag{11}$$

$$\frac{T_1(s)}{I_f(s)} = K_t \tag{12}$$

$$\Delta\theta(s) = \frac{1}{J_{panels}s^2 + c_{panels}s}\, \Delta T_2(s) - \frac{\rho C_m A b V_0}{J_{panels}s^2 + c_{panels}s} \Delta V(s) \tag{13}$$

From these equations, models can be prepared in MATLAB Simulink for simulation. Modelling in MATLAB and Simulink makes the analysis simpler and more effective as changes in parameters or other parts can be evaluated more quickly and accurately than using analytical means. The two Simulink models are shown in Figure 2.9 (a) nonlinear model and Figure 2.9 (b) the linear model.

Following the mathematical model in Simulink simulations ought to be done to study the model behaviour. Parameters like: mass, resistance, inductance, etc. ought to be found, to get these, catalogues will be employed and from these other subsequent parameters will be calculated. All the catalogues used are shown in the Appendices below, these parameters are summarised in Table 1.

2.5 Simulink Model of the nonlinear model

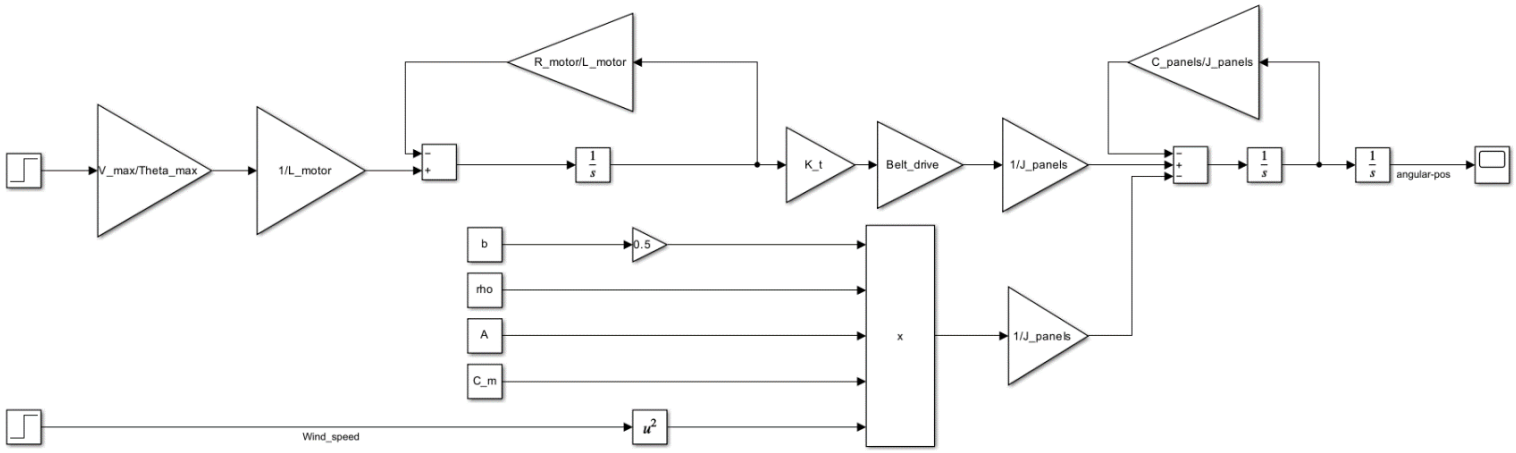

(a)

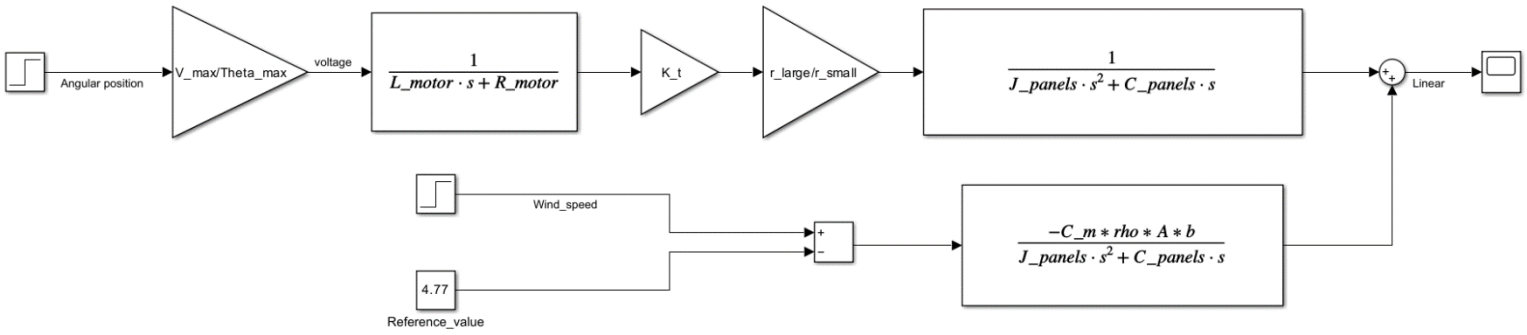

(b)

Figure 2.9: Simulink representation of (a) nonlinear model (b) linear model

Table 1: Model simulation parameters

Property	Symbol	Value
Maximum amplifier voltage	V_{m}	12 V
Maximum amplifier read angle	θ_{max}	2**π** rad
Motor shaft moment of inertia	J_{motor}	0.0425 $kg\ m^2$
Motor coil inductance	L_{motor}	1.066e-03 H
Motor coil resistance	R_{motor}	0.044 Ω
Motor damping coefficient	C_{motor}	0.00025 Nms/rad
Motor torque constant	K_t	0.02271
Pulley radii	r_{large} , r_{small}	0.2, 0.01 m
Panel assembly moment of inertia	$J_{panel}s$	778.5826
Panels damping coefficient	C_{panels}	01005 Nms/rad
Panels drag coefficient	C_m	0.8
Area of panels (maximum taken)	A	13.137 m^2
Air density	ρ	1.225 kg/m^3
Drag moment arm	b	0.944 m

From these values, the system transfer function (without the system architecture) can now be written explicitly for further analysis and simulation of the various system parameters. This transfer function was transferred into a Simulink model and is depicted in Figure 2.10. The transfer function takes in two inputs:

I. The desired solar panel angle as measured by a GPS sensor

II. Wind speed in Sandton

And outputs the actual angle of the solar tracker.

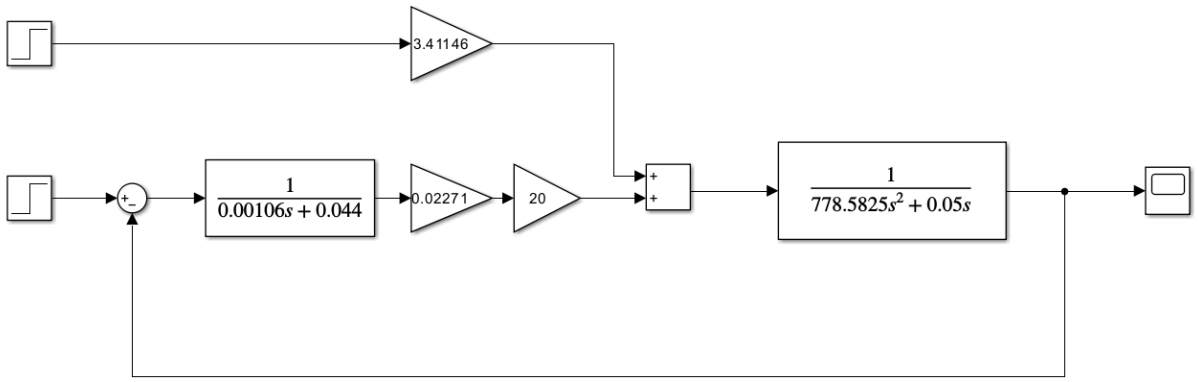

Figure 2.10: Linear transfer function model with numerical values

3 System analysis

3.1 Time-domain response

The time domain response gives us the response of a system as the time varies when a system is subject to some input. The time domain analysis enables us to evaluate specific specifications of the system like the percent overshoot, settling time, rise time, and steady-state error. The response of the system depends on the type of input that the system may be subject to.

3.1.1 Inputs

For the analysis of the solar tracker, the input is the Sun rays' angle as the time varies throughout the day. The rate of change of these is directly linked to the rotation of the Earth in a single day. To choose accurately, select the correct type of inputs to be used for modelling a simple calculation can be made.

$$\text{Suns rays angular rate} = \frac{\text{Earth}_{\text{rev}}}{\text{Time}_{\text{rev}}} \tag{14}$$

Where $Earth_{rev}$ is equal to 360 degrees and $Time_{rev}$ = 86400 seconds. From which the Sun's rays' angular rate can be 0.0042 degrees/s. This rate can be assumed to be constant and linear throughout a 24-hour period furthermore the Sun's direction is always from the East to the West (does not oscillate) and thus for this reason the only two inputs that will be considered for analysis are a **step input** and a **ramp input**.

I. Step input – is a sudden application of the input at a specified time [12].

$$r(t) = A \qquad for\ t \geq 0 \tag{15}$$
$$r(t) = 0 \qquad for\ t < 0$$

II. Ram input – is a constant rate of change in input [12].

$$r(t) = At \qquad for\ t \geq 0 \tag{16}$$
$$r(t) = 0 \qquad for\ t < 0$$

The step and ramp responses are depicted and explained in the subsequent figures, Figure 3.1 and Figure 3.2.

Step input response

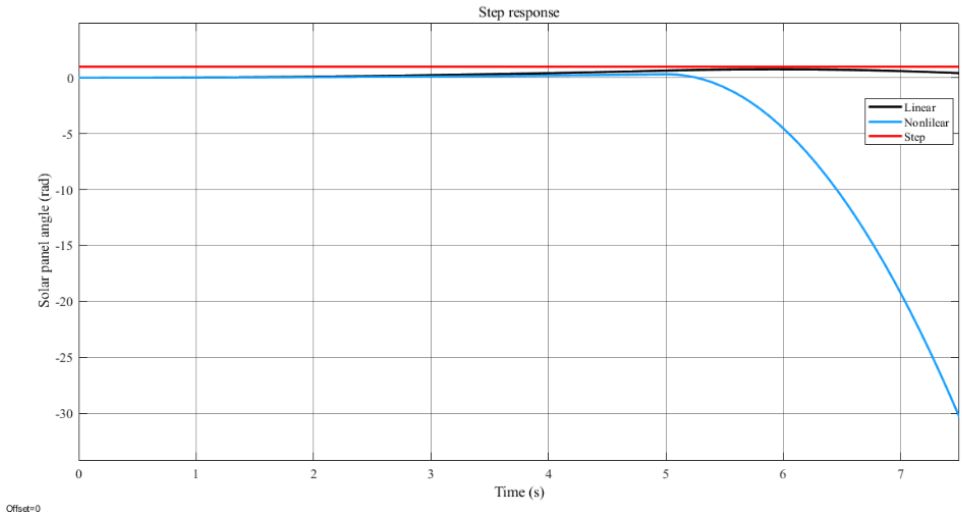

Figure 3.1: Uncontrolled response to a step input

Figure 3.1 shows the uncontrolled linear and nonlinear response of a step input of wind having a speed of 10 m/s. The figure shows that for a step input, the linear and nonlinear system responds similarly because the angular position of both systems have a decreasing angular position which tells us that the solar panels rotate in a clockwise direction (negatively increasing theta) while the nonlinear will rotate faster than the linear system as the nonlinear system reaches -10 radians faster than the linear uncontrolled system does.

Ramp input response

Figure 3.2 below shows the response of the uncontrolled model to a ramp input of the wind speed of 10 m/s. When a ramp disturbance input is introduced, the nonlinear model has a negative decreasing angular position which means that the panel is rotating in a clockwise manner, and it rotates at a faster rate than the linear system rotates. The linear system first rotates in the clockwise direction for the first 4.5 seconds before rotating in the opposite direction (anti-clockwise).

It does not settle to any value, which tells us that the panel just spins around the rotating axis of the system. The nonlinear uncontrolled model responds faster than the linear uncontrolled model.

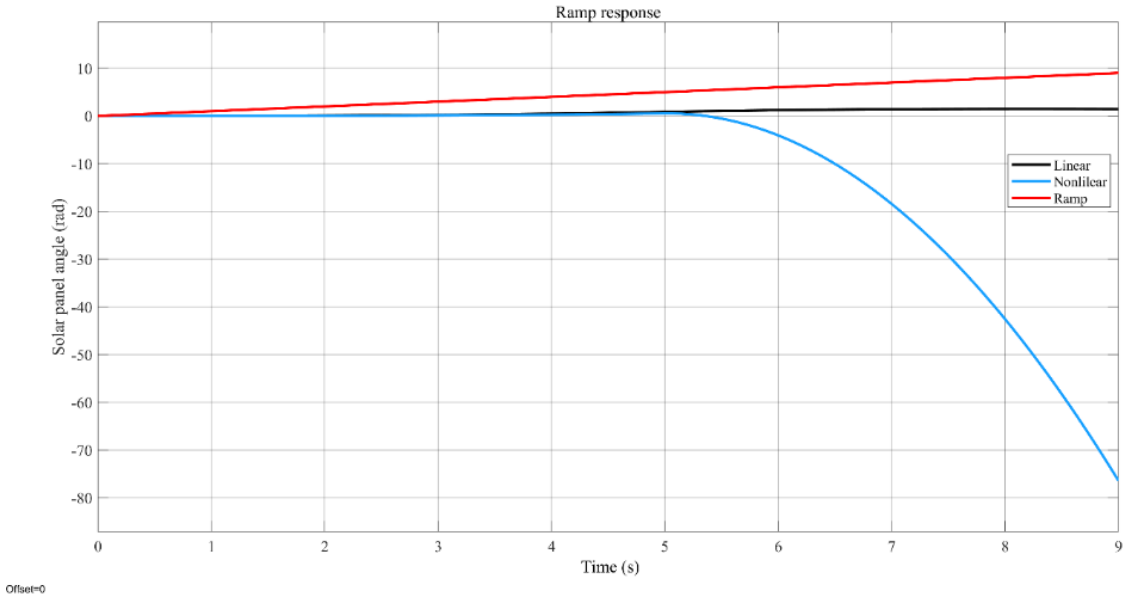

Figure 3.2: Uncontrolled response to a ramp input

3.2 Frequency-domain response

To describe a linear system's response in the frequency domain, bode plots are employed. Bode plots provide information about the system change in Magnitude and phase gain plotted against frequency. This information is useful when it comes to determining the stability of the system. A Bode plot was constructed to determine the frequency response of the system. The frequency response of the linear system, in Figure 3.3 shows the magnitude and phase changes against the frequency. The gain margin is calculated from the magnitude plot, while the phase margin is calculated from the phase plot. Both the phase and gain margins are zero for the system. This is an indication of marginal stability. Any changes in the system's parameters will result in instability.

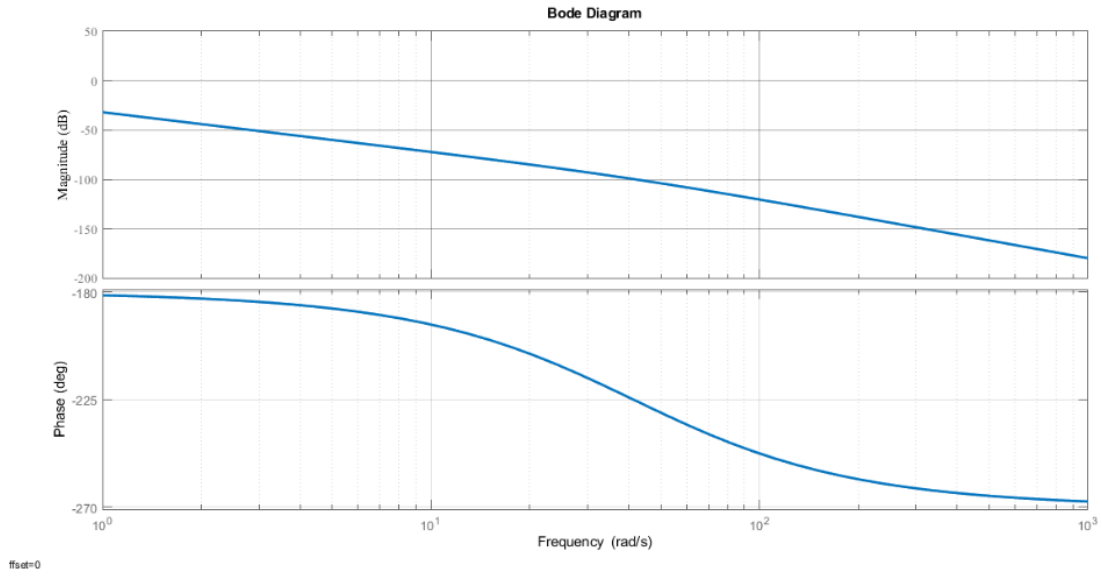

Figure 3.3: Bode diagram of the linear uncontrolled plant

4 Stability analysis

4.1 Linear stability analysis

4.1.1 Routh Hurwitz Criterion

The Routh Hurwitz criterion for stability is a method used to determine the stability of a closed loop system by determining the number of poles of the system that are in the left half plane, right half plane, and the imaginary axis of the s-plane (i.e. complex plane). A Routh Table is generated by using the transfer function of the closed-loop system. The number of poles in the right and left plane is determined by the number of sign changes in the first column of the Routh Table. The number of poles in the imaginary axis is determined by the roots that lie on the imaginary axis. The system is thus considered stable if the first column has zero sign changes with all variables being positive and has all the poles in the left half plane.

The transfer function of the closed-loop system for the solar panel system is given by:

$$P(s) = s^3 + 41.28\, s^2 + 0.002651 s + 1 \qquad (17)$$

Table 2: Routh array for the solar panel system

s^3	1	0.002651
s^2	41.28	1
s^1	−0.0227	
s^0	1	

The first column of Table 2 has two sign changes from +41.28 to – 0.0227 and then from -0.0227 to +1. Thus, from this observation from the Routh array, there are two poles that exist in the right half plane and one on the left-hand plane pole, thus according to the Routh-Hurwitz criterion the system can be deemed unstable.

4.1.2 The Pole Zero plot

The pole-zero plot depicts the location of poles and zeros of a transfer function for a closed-loop system in the s-plane (i.e. complex plane). The plot can be carried out in MATLAB where the poles are shown by X and zeros are shown as O on the complex plane. The location of poles can be visualized from the plot thus enabling the determination of the number of poles in the left-hand plane, the right-hand plane, and the imaginary axis of the s-plane.

The poles of the system are plotted in Figure 4.1, showing their locations on the S-plane. One pole exists on the left-hand plane of the s-plane, and two exist on the right-hand plane.

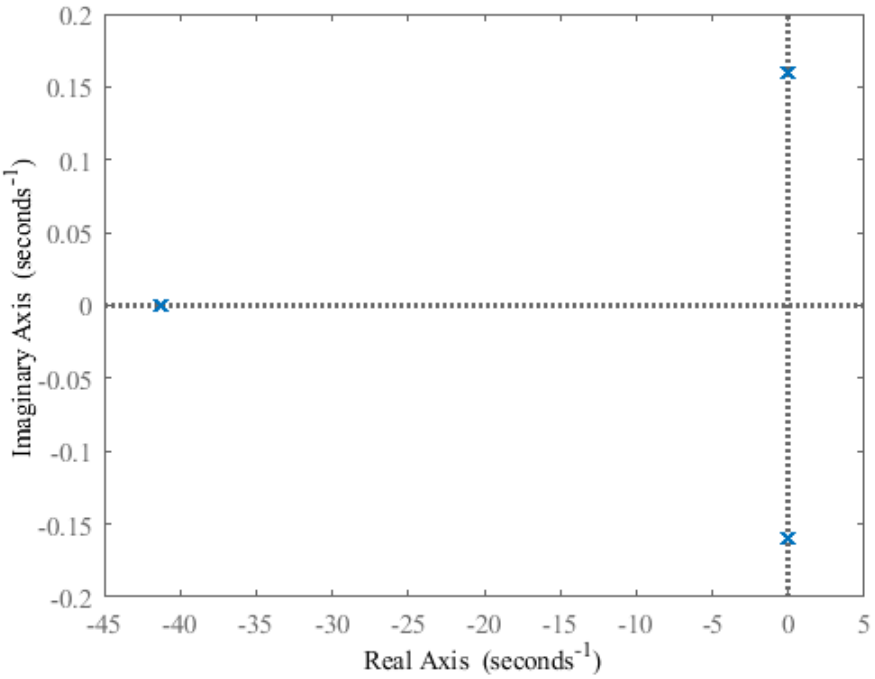

Figure 4.1: The Polar Zero plot of the solar panel closed loop system.

4.2 Controller necessity

From several tools including, the time response of the system, frequency response, pole-zero plot, and the Routh Hurwitz method that were used it is obvious that the system is operating between marginal stability and instability. This means that the system will break apart, destroy some or all its components or potentially be a danger to users, and pose a risk to the environment. Consequently, this means that the system will not perform within the required specifications. This will be an unusable system as it will not be able to achieve what it is designed to achieve. For these two reasons, a controller is suggested to be incorporated into the system to ensure that the system is stable and efficient.

5 Controller implementation

5.1 Performance specifications

In attempting to design controller, specifications are vital in providing quantitative measures of the dynamic behaviour. Specifications for control design can be in the time domain (which includes, percent overshoot, rise time, settling time, and steady-state error) or in the frequency domain (gain margin, phase margin, and bandwidth). These specifications offer insights into system performance. The meanings of these specifications are explored now is the following subsections.

5.1.1 Percent Overshoot (M_p)

Percent overshoot is a measure of how much a system's response exceeds its steady-state value in percentage terms. For a solar tracker, percent overshoot influences the oscillations experienced during the tracking process as it adjusts its position to follow the Sun's movement. Minimizing percent overshoot is crucial to ensure smooth and efficient solar tracking, thereby maximizing energy capture.

5.1.2 Rise Time (T_r)

Rise time represents the time taken for the system's response to rise from a specified lower threshold to a specified upper threshold for the first time. For a solar tracker, shorter rise time means quicker repositioning in response to changes in solar position, enabling the system to accurately track the Sun's movement and optimize energy capture efficiency.

5.1.3 Settling Time (T_s)

Settling time refers to the time required for the system's response to reach and remain within a specified percentage (typically 2-5%) of its final value after a disturbance or change in input. In the context of a solar tracker, minimizing settling time is essential to ensure prompt and accurate repositioning after disturbances, thereby reducing tracking errors and maximizing energy harvesting efficiency.

5.1.4 Steady-State Error (e_{ss})

Steady-state error is the difference between the desired and actual values of the system's output once the transient response has settled. For a solar tracker, minimizing steady-state error ensures accurate positioning relative to the Sun over extended periods, maximizing energy generation performance and overall system reliability. These are summarized in Figure 5.1 below:

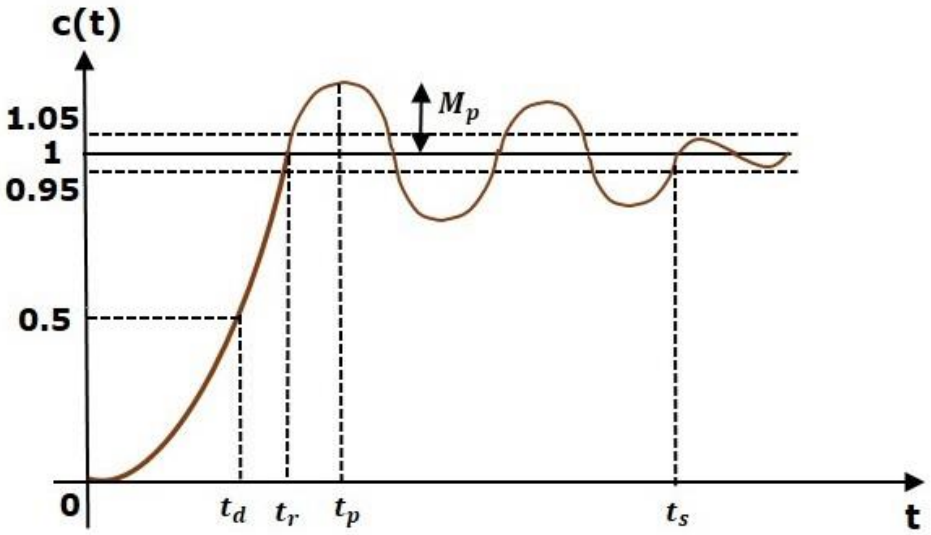

Figure 5.1: Diagrammatic representation of time domain specifications [14]

5.1.5 Gain margin

Gain margin is a measure of how much the gain of a system can be increased before it reaches instability, typically expressed in decibels (dB).

5.1.6 Phase margin

Phase margin shows how much additional phase shift can be tolerated in the system before it becomes unstable.

5.1.7 Bandwidth

The bandwidth is the range of frequencies for which the normalized gain of the system is more than -3 dB. The bandwidth is the measure of the ability of a feedback system to reproduce the output signal, and noise rejection characteristics over time. These are represented diagrammatically in Figure 5.2 below. From the above-discussed and represented time and frequency domain specifications, the specifications that the system is required to have are summarized in Table 3 and

Table 4 below. These specifications will ensure that the system is stable and tracks the Sun to within the desired performance criteria.

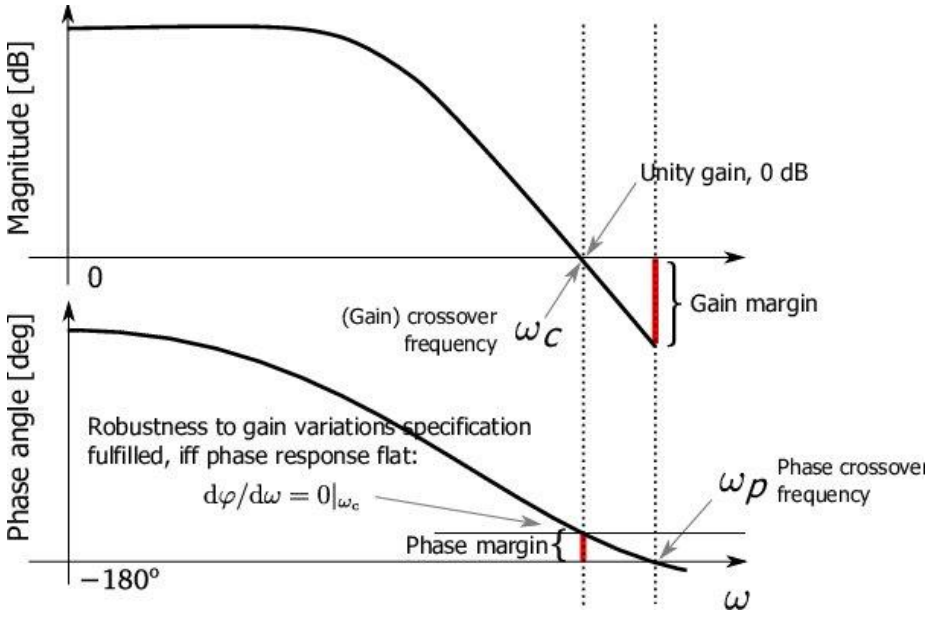

Figure 5.2: Frequency domain specifications showing gain and phase margins [15]

Table 3: Time-domain specifications

Specification	Symbol	Value
Percent overshoot	$\% OS$	$10\ \%$
Rise time	T_r	$1\ s\ <$
Settling time	T_s	$2.5\ s\ <$
Steady state error	e_{ss}	0

Table 4: Frequency-domain specification

Specification	Symbol	Value
Gain margin	$\% OS$	$> 6\ dB$
Phase margin	T_r	$> 40^{\circ}$
Bandwidth	T_s	$300 \frac{rad}{s} <$

5.2 Root locus control technique

The root locus is a graphical method used in control theory to analyze how the roots of a system's characteristic equation vary with changes in a specific parameter, usually a controller gain. It helps visualize how the systems' stability and transient response change as this parameter is adjusted. The root locus represents the paths taken by the roots in the complex plane as the parameter varies, providing insights into the systems' behavior and aiding in controller design. This control technique is now used to design a feedback control system. The architecture of the control system is summarised in Figure 5.3 below.

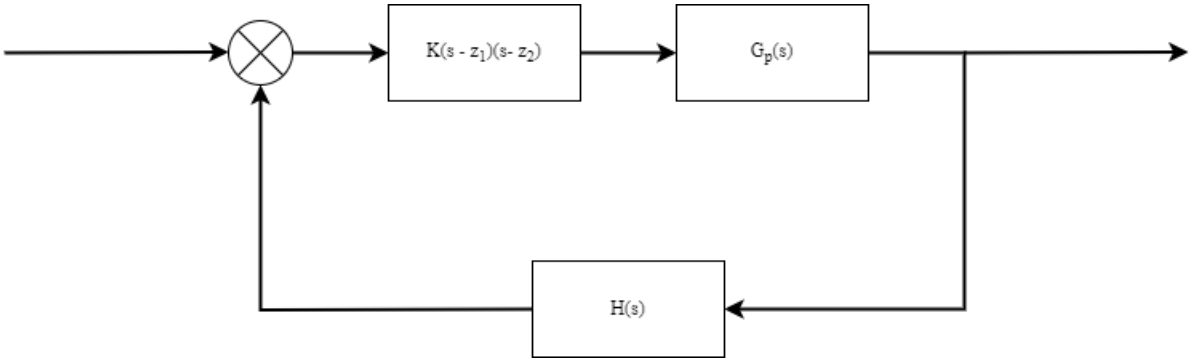

Figure 5.3: Control architecture for the root locus

The steps to be used to design the root locus control technique for the plant are summarised below:

Step 1: Launch the Control System Designer from MATLAB command: controlSystemDesigner(TF), where TF is the transfer function being analysed.

Step 2: Set the design specifications required for the performance of the system. This creates the design point (the point the root locus is supposed to pass for the system to behave as required).

Step 3: Usually, the system will not pass through the design point. In such a case either a pole(s) or zero(s) or both can be added to the system to alter the root locus such that it passes through the design point.

Step 4: After the addition of the pole(s) or the zero(s) the gain is either increased or decreased until the design specifications are met and if not, the location of the pole(s) or zeros (s) is revised and the gain either increased or decreased until the specifications are met. This is process is also referred to as tuning the controller.

Step 5: After the tuning, a transfer function is produced which is then cascaded with the main plant and is controlled in that way.

The above-suggested process is adopted and used for the control of the controller.

```
Command Window
fx >> controlSystemDesigner(Transfer_func)
```

Figure 5.4: Command to launch the control system designer in MATLAB

Using the transfer function of the plant that has been provided from Figure 2.10, the root locus can be found using the command given in Figure 5.4 and for the uncontrolled plant, the root locus is depicted in Figure 5.5. The root locus has its parts on the right half plane naturally and will only be between marginal stability and instability for any value of "K" and thus modifications to the root locus ought to be done.

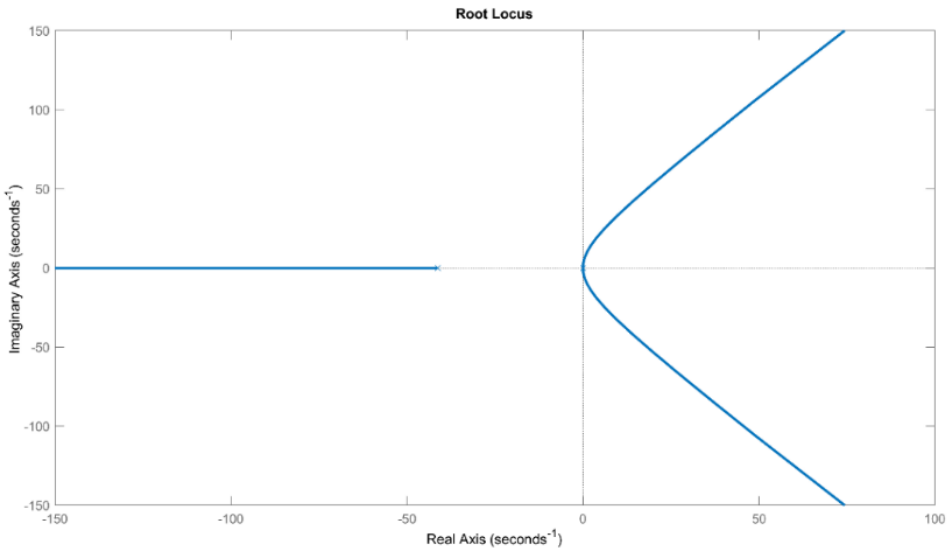

Figure 5.5: Root locus of the uncontrolled plant

The literature from [12] suggests two ways of stabilising and controlling a system using the root locus and these are briefly discussed:

I. Add a pole to the root locus – adding a pole to the root locus shifts the entire root locus to the right, depending on where the root locus is located – the system can become unstable if poles lie in the right half plane.

II. Add a zero to the root locus - adding a zero to the root locus shifts the entire root locus to the left, depending on where the root locus is located – the system can become stable if zeros lie in the left half plane.

Thus, for the reasons above, to stabilise the system and control it so that it meets the performance specifications two zeros must be added to the system as the controller and the architecture is shown in Figure 5.6 below.

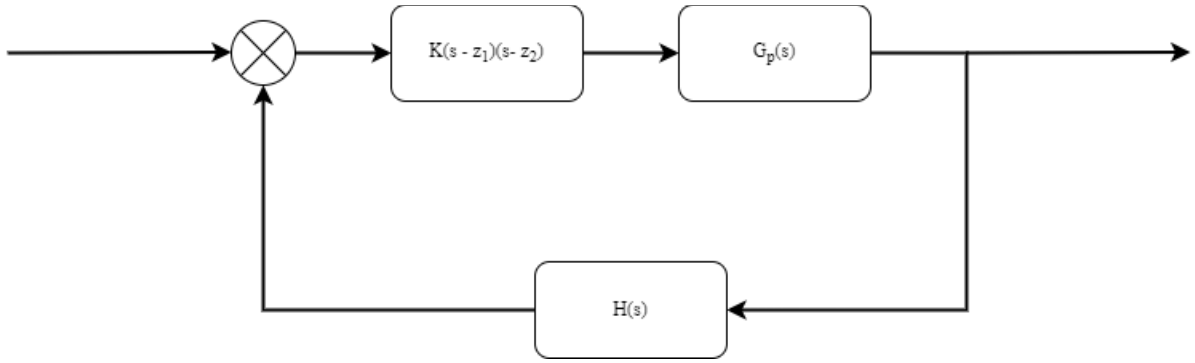

Figure 5.6: Controller architecture for the root locus controller

The two zeros added were: z_1 = -2 and z_2 = 30, the gain value was varied and the gain value "K" that met the performance specifications was selected as K = 12. The new transfer function was found by cascading the plant with the newly designed root locus controller and is shown in Figure 5.7 below.

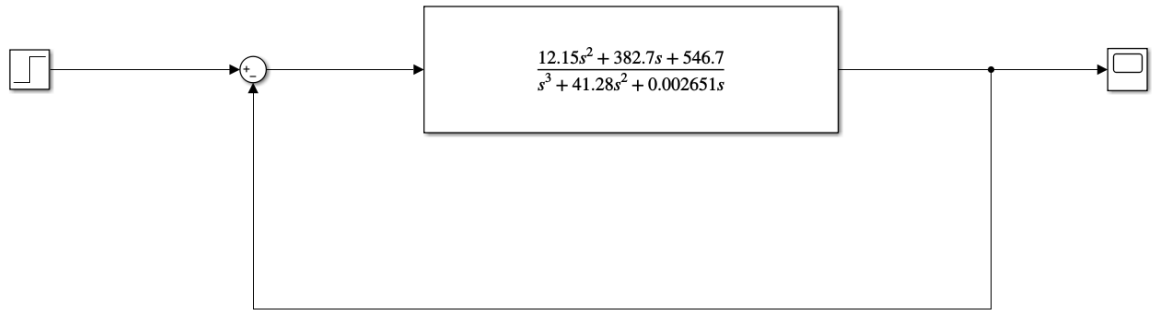

Figure 5.7: Root locus-controlled plant transfer function

The corresponding root locus response of this new system with two poles is show below in Figure 5.8.

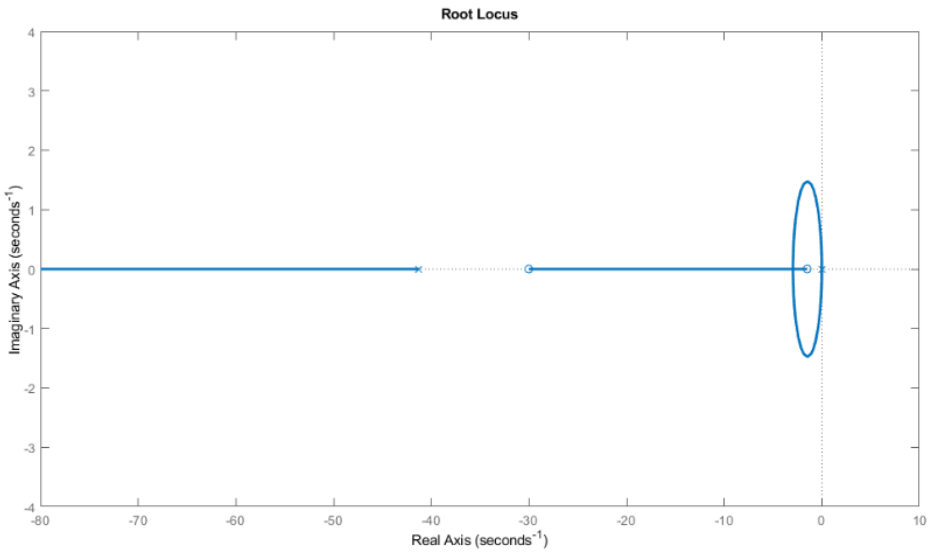

Figure 5.8: Root locus of the newly designed controller cascaded with the plant

This root locus plot is different from the uncontrolled plant, since for any gain value ($0 < K < \infty$) the system is always stable. The time response of the root locus-controlled plant to both a step and a response input is now explored. The time response of the root locus-controlled plant to a step is depicted in Figure 5.9 and to a ramp input is depicted in Figure 5.10.

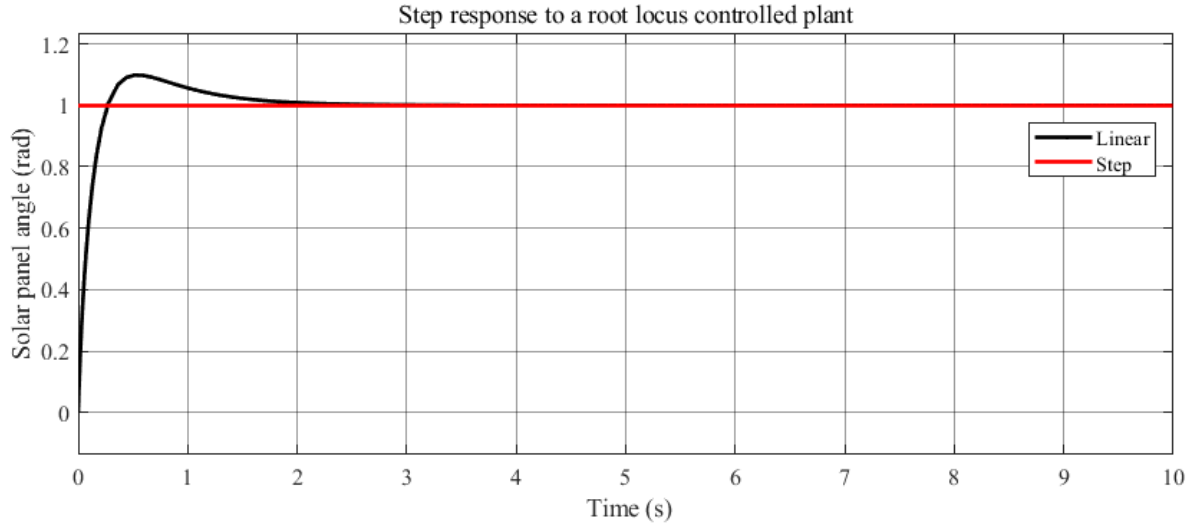

Figure 5.9: Root locus response-controlled plant to a step input

Figure 5.9 above shows that the system is stable. The rise time is about 0.3 s (below 1 s), the percent

overshoot is about 9% and the settling time is about 2 seconds (which is exactly the one that was required. The system has a zero steady state error. The linear system whose controller has been designed using the root locus method can be assumed to be performing within the required time-domain specifications. In Figure 5.10 the root locus controller also performs well for a step response with all the error disappearing after a time of about 1 s.

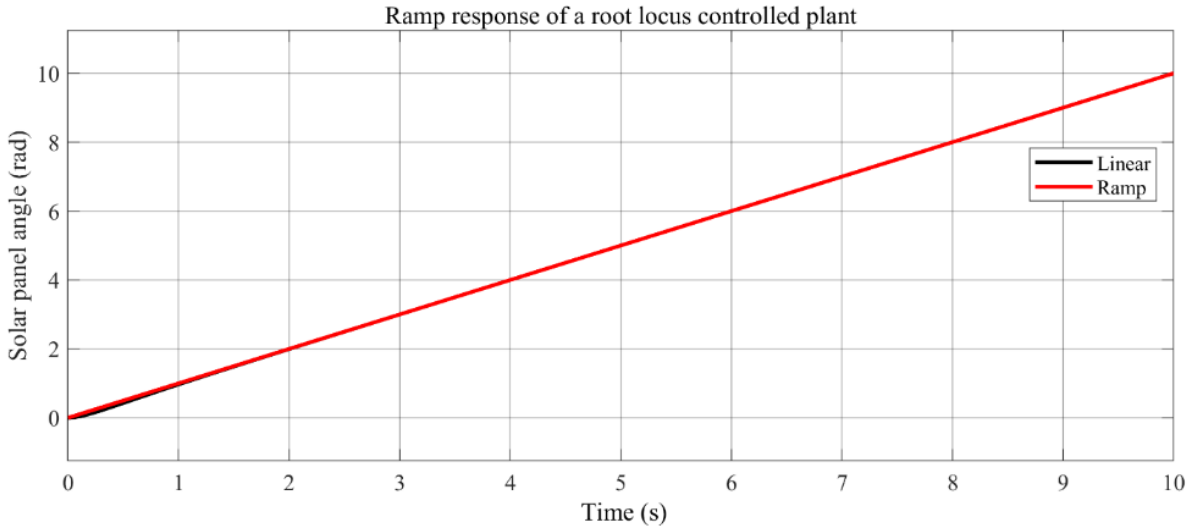

Figure 5.10 Root locus response-controlled plant to a ramp input

5.3 Proportional Integral Derivative (PID) control technique

A PID controller is a feedback control mechanism widely used in engineering and automation to regulate systems and processes. Its acronym stands for Proportional, Integral, and Derivative, representing the three primary control actions it employs. The control law governing a PID controller is summarised by the equation:

$$U(t) = K_p\, e(t) + K_i \int_0^t e(z)dz + K_d \frac{de}{dt} \qquad (18)$$

The proportional (K_p) component generates an output signal that is directly proportional to the current error signal. The proportional action provides immediate corrective action based on the magnitude of

the error, aiming to reduce it quickly.

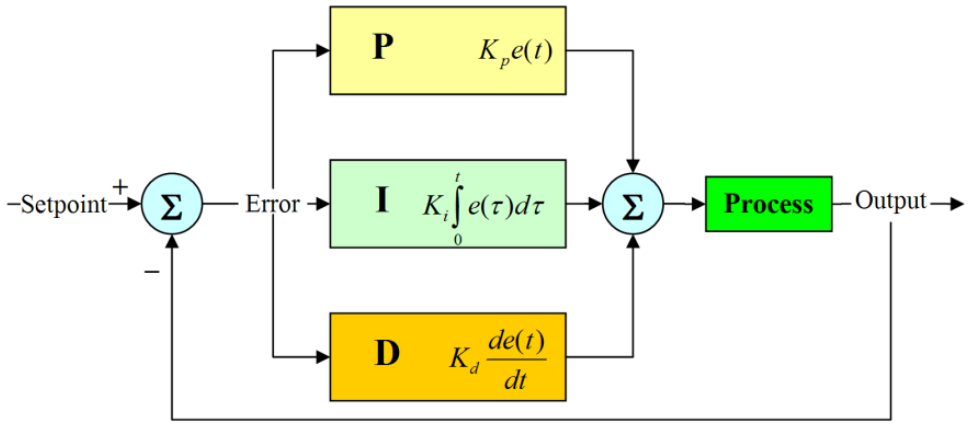

Figure 5.11: PID control law block diagram [16]

The integral (K_I) component integrates the error signal over time, effectively accumulating the historical error. It produces an output signal proportional to the integrated error, which allows the controller to eliminate any steady-state error that remains after the proportional action. The derivative (K_D) component responds to the rate of change of the error signal. It calculates the derivative of the error with respect to time and generates an output signal proportional to this rate of change. The derivative action provides anticipatory control, damping the system's response to rapid changes in the error signal and improving stability by reducing overshoot and oscillations [16].

To tune the PID controller, the PID tuning app will be used.

Using the steps above, the controller gains were determined have the values:

- K_p = 608
- K_i = 125
- K_d = 460

All these PID gains were selected from the tuning of the controller using the PID Tuner App in Simulink and these achieved the performance specifications with a filter coefficient for the derivative gain value of N = 1289.

5.3.1 Time response of PID controller

From Figure 5.12 below, the systems can be said to be stable for both the linear and the nonlinear case. The rise time is about 0.2 s (also below 1 s), the percent overshoot is about 9% and the settling time is about 2.15 seconds (which is exactly the one that was required). The system has a zero steady state error. The linear system whose controller has been designed using the root locus method can be assumed to be performing within the required time-domain specifications. These are the performance specifications for standard conditions in Sandton – with a wind of about 4.77 m/s.

For further understanding of the controller performance the wind speed was increased to measure the systems robustness. Figure 5.13 (a) shows the controller response to a wind speed double that of standard conditions (about 10 m/s the wind speed). From that plot the linear and nonlinear plots still respond similar as in the standard conditions case. The nonlinear model has characteristics that are lower than the linear model – slightly lower percent overshoot, lower rise time. The nonlinear model however has a non-zero steady state error which continues beyond the 10th second of signal application. This is similar for even higher wind speeds (about 5 times the standard conditions – 25 m/s wind) where the effects are amplified from that case of a wind speed of 10 m/s.

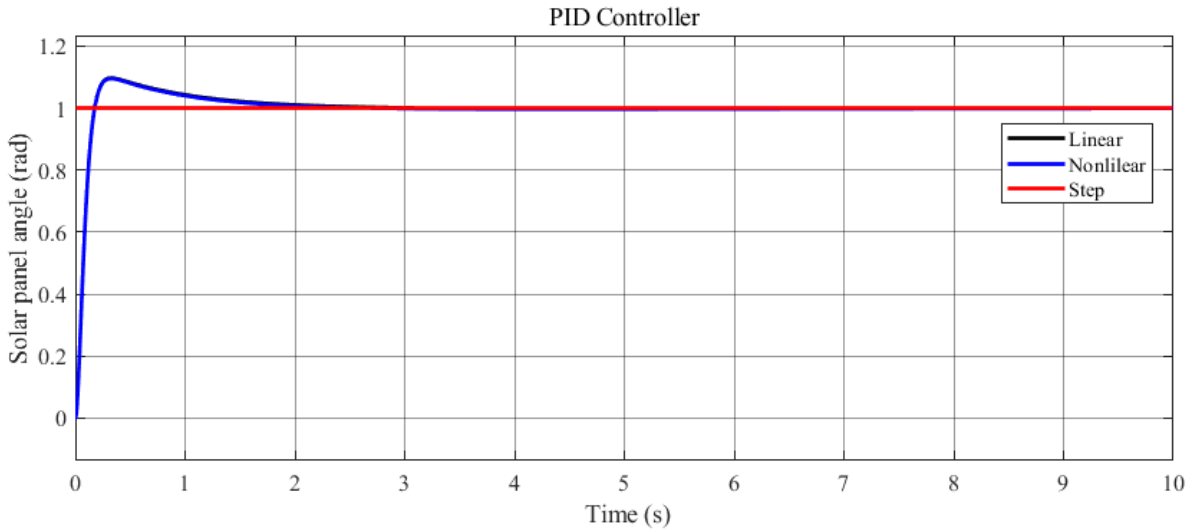

Figure 5.12: PID controller for the plant

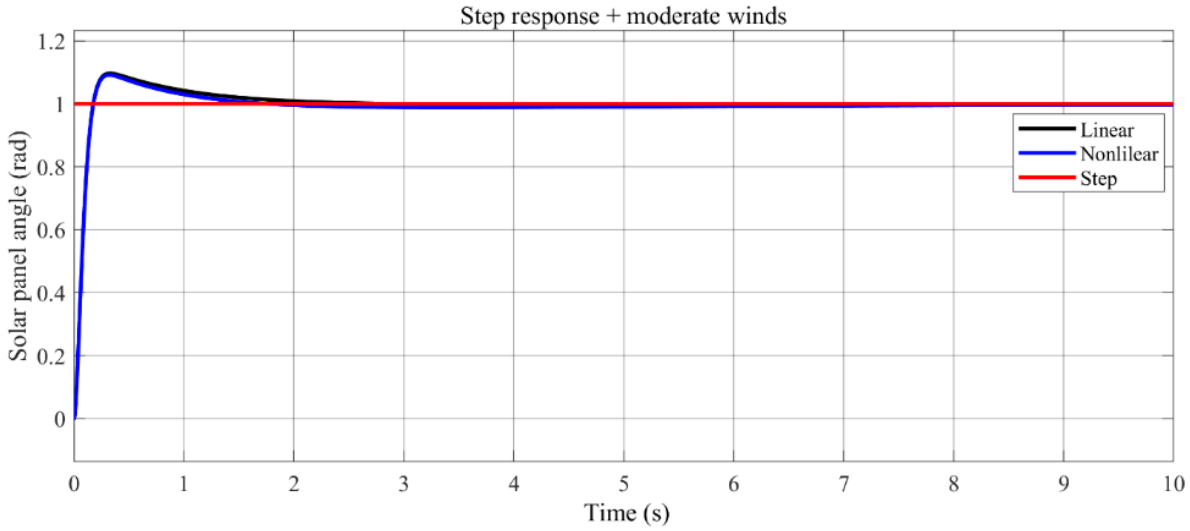

(a)

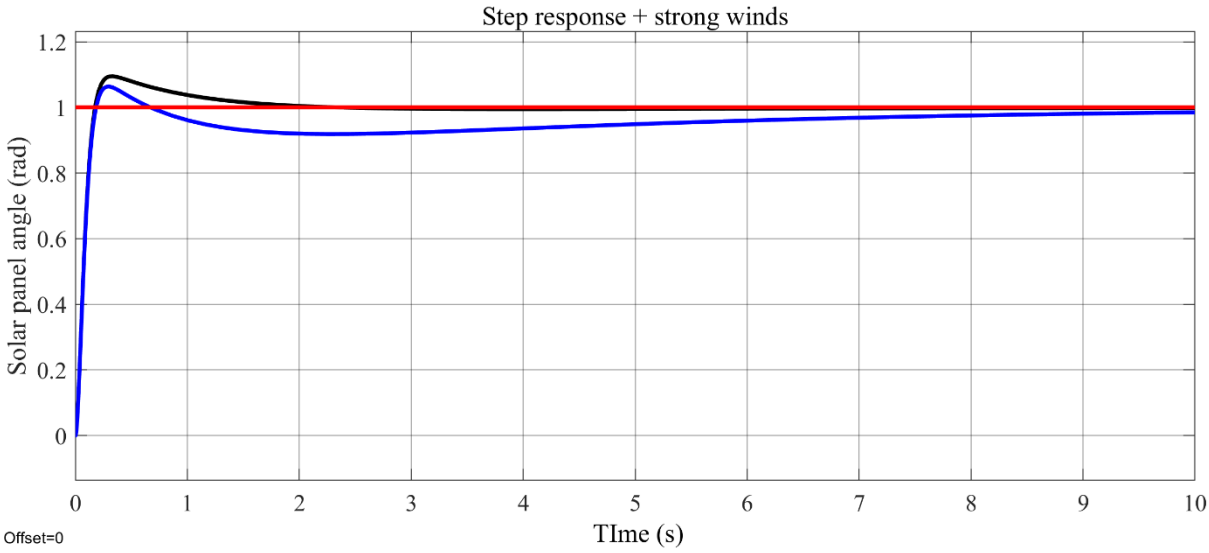

(b)

Figure 5.13: Solar panel variation with increasing wind speeds (a) speed of 10 m/s (b) 25 m/s

5.3.2 Frequency response of the PID controller

The frequency response of the PID-controlled system is shown in the Bode plot in Figure 5.14: Bode diagram for the PID-controlled system. The minimum gain and phase margins required for the system to reach stability are 6dB and 40 degrees, respectively. The gain and phase margins of the controlled system are +45 dB and +60 degrees, respectively. The positive signs of the margins indicate that the system is stable. Furthermore, the margins are significantly greater than the minimum required margins. Thus, the system is stable, robust, and can withstand disturbances without compromising the stability of

the system. The implemented control was sufficient.

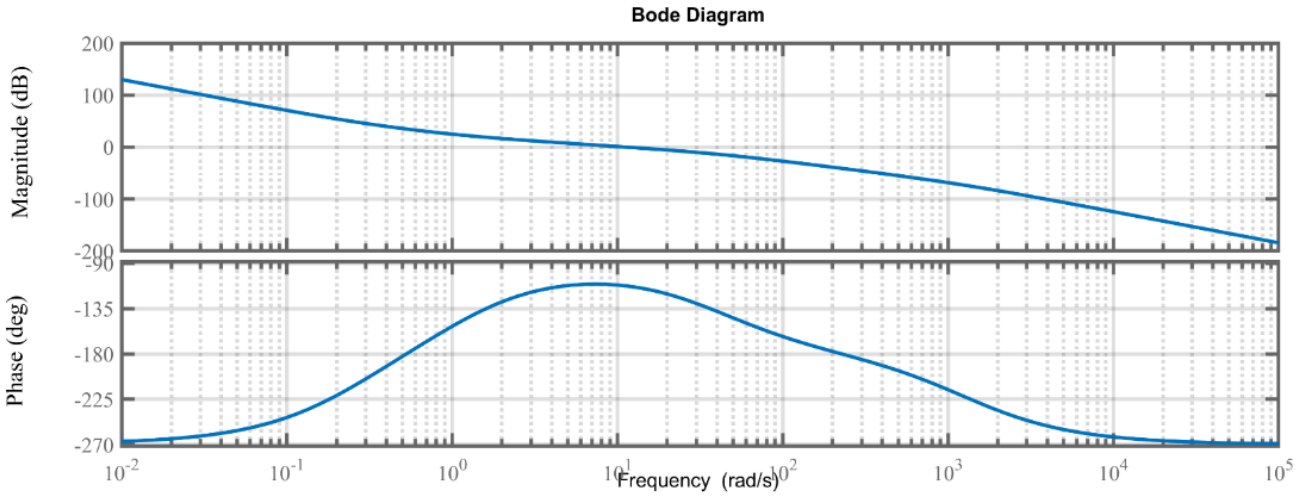

Figure 5.14: Bode diagram for the PID-controlled system

5.4 Controller implementation in the Winter and in Summer conditions

With the controllers developed above, the system can be tested on the operations of a single day in winter and a single day in summer. To do this – it is assumed that this controller is incorporated with a Global Positioning System (GPS) device that is capable of reading and producing the Sun's movement in a single day based on that specific day of the year and from some predetermined time (based on the expected Sunrise expected Sunset times). The GPS Sun tracker will be developed based on the latitude of Sandton amongst other factors. The GPS Sun tracker uses the following information to track the Sun [17]:

I. Sun's declination angle - the angle between the Sun's direction and the equatorial plane, this angle calculation is given by the equation:

$$\delta = 23.45° \sin\left[\frac{360}{365}(n + 284)\right] \tag{19}$$

Where δ is the Suns' declination angle and n is the day in the year ($n = 5$ means $5\ January$).

II. Hour angle – this is the angle through which the Earth has rotated since solar noon. This angle is given by the equation:

$$h = (local\ time - 12) * 15° \quad (20)$$

III. Solar altitude angle, α - The angle between the solar beam and the horizontal. This angle is given by the equation:

$$sin\alpha = sinL_S\ sin\delta + cosL_S\ cos\delta\ cosh \quad (21)$$

Where L is the local latitude for the area in question, in this case $L_S = 26.1076°$ S latitude.

IV. Angle of incidence of the Suns rays - the angle between solar beam and surface normal.

$$cos\theta = sinL_S sin\delta cos\beta - cosL_S\ sin\delta sinB cosZ + cosL_S\ cos\delta coshcos\beta + \cosh sin\beta\ cosZ_S + cos\delta \sinh sin\beta\ sinZ_S \quad (22)$$

From this set of equations, the Sun's path for two days (one in winter and one is summer) can be traced and plotted down in a curve. The Sun's angular position will then be plotted as the time varies and thus used as the input signal into the solar tracker control system. The angle of incidence given by equation (19) produces values that are negative from Sunrise to noon and positive from noon to Sunset. This is depicted in Figure 5.15 below.

As the Sun rises in the early AMs, the angle of incidence will be negative, the solar panel will have a zero angular displacement value and as soon as the Sun starts beaming sufficient rays the solar tracker gets active, this is usually about 06:00 AM. To simulate this solar tracking phenomenon, a script was prepared in MATLAB. This script serves as a representation of the GPS sensor that will feed the desired angular position to the solar tracker and the Sun will be tracked. This solar tracker script is prepared and presented in Appendix B.2, the script was prepared using literature in [17] and adapter for use in this paper. Two dates were chosen for simulation – these dates are 21 June, which is regarded as mid-winter [18] and 21 December, which is regarded as mid-summer [19]. Figure 5.16 (a) shows the simulated results of the Sun path in summer (21 December) and Figure 5.16 (b) shows the simulated results of the Sun's path in winter (21 June). The PID-controlled solar tracker seems to be swiftly following the Sun's angular position from Sunrise (at about 06:00 AM) till noon (at about 16:00). The solar tracker can be taken to perform within the required performance specifications.

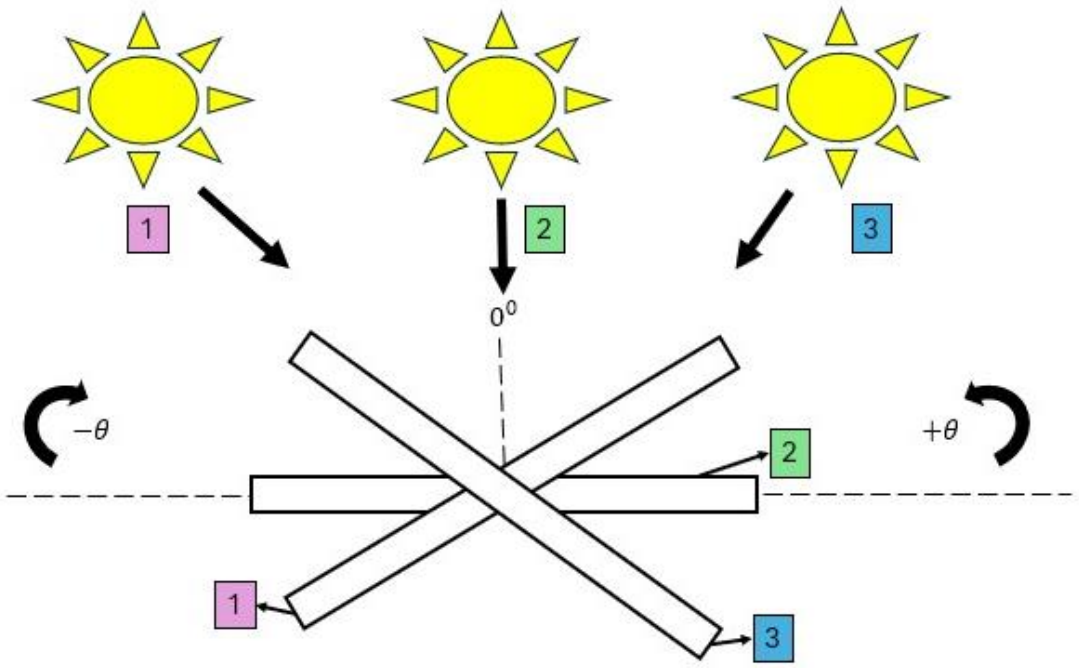

Figure 5.15: Movement of the Sun and reaction of the solar panel

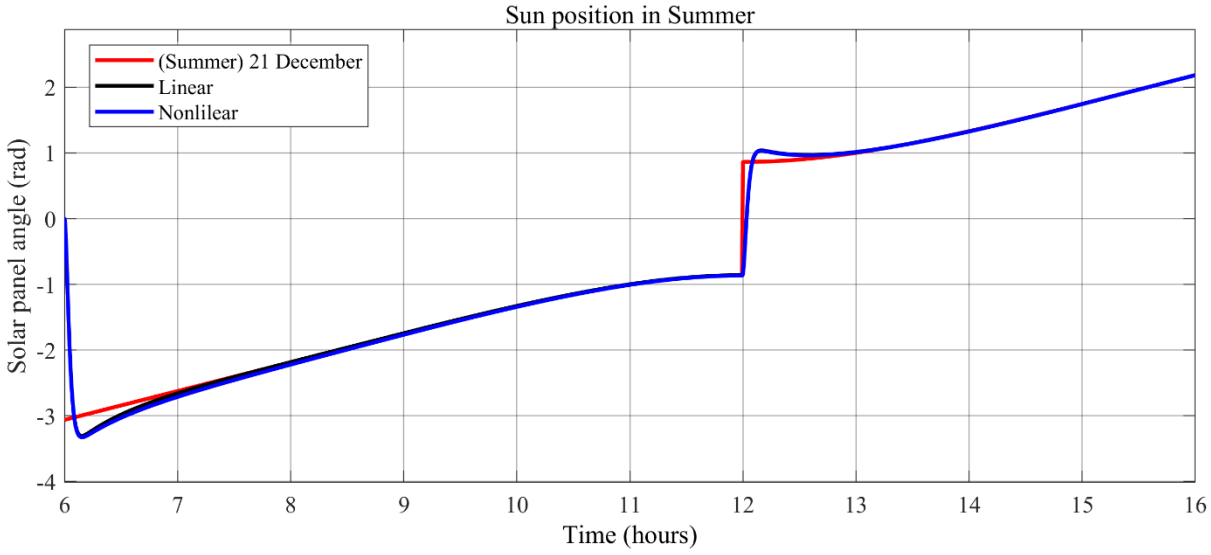

(a)

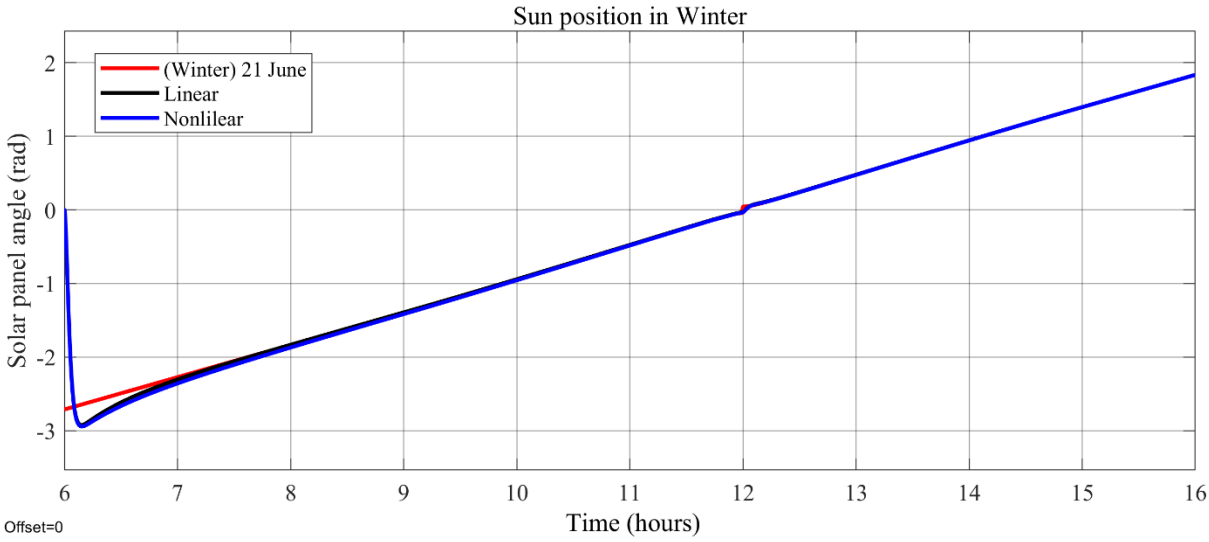

(b)

Figure 5.16: Suns path and tracking with PID of the linear and the nonlinear in (a) Summer and (b) Winter

6 Discussion and conclusion

This paper aimed to model and control the behaviour of a solar tracker system. The steps followed here are the steps of a dynamic investigation which are [6]: physical modelling, mathematical modelling (differential equations), behaviour analysis, and decision design. Based on this, a mathematical model was developed (linear nonlinear) from which simulated time and frequency responses were prepared. Based on the time response and the frequency response (bode plot) it was deemed that the model linear and nonlinear models were not converging to some specified value. Then, stability analysis techniques were used to further investigate the behaver of the system. In this Routh-Hurwitz and the Pole-Zero plot from these techniques, it was immediately concluded that the system model was unstable and thus uncontrollable. For this reason, a controller was deemed necessary for use in this system.

In designing any controller, some expected system behaviour needs to be specified. The specifications that this solar tracker needed to adhere to are a percent overshoot of 10%, a settling time of less than 2.5 s, a rise time of less than 1s and a zero steady-state error in the time domain. In the frequency domain, the system was required to have a gain margin greater than 6 dB, a phase margin greater than 45 and a bandwidth greater than 30 rad/s. From, two controller design techniques were selected for use: the root locus control design and the Proportional, Control, and Derivative (PID) control design technique.

A root locus control design technique makes a graphical representation of the closed loop poles as the gain value “K” is increased. Two of these were created, a root locus for the uncontrolled system and one for the controlled system. The root locus for the uncontrolled system crossed the imaginary axis and proceeded to the right half plane further confirming instability.

For a permanently stable system, the root locus needs to not cross the imaginary axis, in order to do this, one can add either poles or zeros in the system. Adding poles to the system shifts the entire root locus to the right, whereas adding zeros to the system shifts the entire root locus to the left [12]. For this reason, two zeros (one at -30 and one at – 2) were added to the system making the entire system stable, furthermore to the permanent stability of the system, the specifications need to be met. In order to meet the specifications, the gain value was increased from zero, and at a gain value of about 12.7 the system showed approximately the desired behaviour. From the performance specifications of the root locus in sections 5.2 it can be said that the root locus controller can be used for control of a linear system. The PID controller was then designed following the root locus-designed controller.

A PID controller was developed in the immediately following section 5.3. The PID controller was tuned using the PID tuning App in Simulink from which the K_p, K_I and K_d gains were then generated by the PID tuning app and adapted for use in the system. The K_p, K_I and K_d values were 608, 125 and 450

respectively. The PID controller was able to stabilise the system, furthermore the system had an overshoot of about 9%, a settling time of 2.15 s, a rise time of about 0.2 s and a zero steady state error for the standard conditions of Sandton area. This means that the PID controller can be effectively used the control the solar tracker for efficient energy harvesting in Winter and in Summer.

6.1 Instrumentation Needed To Apply.

The primary objective of the mechatronic system is to track the Sun's position and adjust the solar panels' position. The Sun’s position can be complex to measure and predict because atmospheric conditions change with seasons. However, at any point, the solar panels' photovoltaic cells detect the UV-rays. The amplifier uses the information from the photovoltaic cells and the panels' orientation to send signals to the control system (PID controller). The control system sends signals to the motor, which will turn the belt system. Thereby adjusting the orientation of the solar panels to optimal alignment. This way, the solar panels are always perpendicular to the Sun’s rays, and the efficiency of harvesting solar energy is increased.

References

[1] Khalil FA, Asif M, Anwar S. Solar Tracking Techniques and Implementation in Photovoltaic Power Plants: a Review. Pak Acad Sci n.d.

[2] Where is Sandton, South Africa on Map Lat Long Coordinates 2024. https://www.latlong.net/place/sandton-south-africa-2210.html (accessed May 7, 2024).

[3] Sandton climate: Weather Sandton & temperature by month n.d. https://en.climate-data.org/africa/south-africa/gauteng/sandton-27317/ (accessed May 7, 2024).

[4] Elevation of Sandton,South Africa Elevation Map, Topography, Contour n.d. https://www.floodmap.net/elevation/ElevationMap/?gi=957654 (accessed May 7, 2024).

[5] Simulated historical climate & weather data for Sandton. Meteoblue n.d. https://www.meteoblue.com/en/weather/historyclimate/climatemodelled/sandton_south-africa_957654 (accessed May 7, 2024).

[6] Panday A. MECN4029A MECHATRONICS II. Univ Wiwatersrand 2024.

[7] Servo drive. Wikipedia 2023.

[8] MCP41010-E/P, Digital Potentiometer 10kΩ 256-Position Linear Serial-SPI 8 Pin, PDIP | RS n.d. https://za.rs-online.com/web/p/digital-potentiometers/0403676 (accessed May 7, 2024).

[9] Controlling and Troubleshooting Common DC Motors - Technical Articles n.d. https://control.com/technical-articles/controlling-and-troubleshooting-common-dc-motors/ (accessed May 7, 2024).

[10] Belt Drive Design Fundamentals for Industrial Applications Webinar n.d. https://www.wmberg.com/resources/webinars/when-is-a-belt-drive-better-for-mechanical-power-t (accessed May 7, 2024).

[11] Shukla S. Optimal solar panel configuration Archives. Fenice Energy 2024. https://blog.feniceenergy.com/tag/optimal-solar-panel-configuration/ (accessed May 7, 2024).

[12] Bakshi U. Control Systems Engineering 2020.

[13] Ngo XC, Nguyen TH, Do NY, Nguyen DM, Vo D-VN, Lam SS, et al. Grid-Connected Photovoltaic Systems with Single-Axis Sun Tracker: Case Study for Central Vietnam. Energies 2020;13:1457. https://doi.org/10.3390/en13061457.

[14] Time Domain Specifications. TutorialspointCom 2024. https://www.tutorialspoint.com/control_systems/control_systems_time_domain_specifications.htm (accessed May 4, 2024).

[15] Tepljakov A, Petlenkov E, Gonzalez E, Petráš I. Design of a MATLAB-based teaching tool in introductory fractional-order systems and controls. Technical University of Kosice; 2017. https://doi.org/10.1109/FIE.2017.8190681.

[16] Charlotte. PID Control 2022. https://eng-resources.charlotte.edu/unccengkit/coding/pid-control/ (accessed May 7, 2024).

[17] Akram Adbulameer AA-K. A comprehensive solar angles simulation and calculation using MATLAB. Int J Energy Environ 2015.

[18] Winter solstice. Wikipedia 2024.

[19] December 21. Wikipedia 2024.

Appendix

A Parameter calculations

Moment of inertia of solar panel

$$J_{panels} = \frac{1}{12} M_{panels} (a^2 + b^2)$$

$$J_{panels} = 778\, kg.m^2$$

Contrast value of solar panel area – A

$$A = b * h$$

$$A = 13.13\, m^2$$

B MATLAB codes

B.1 Solar panel parameters

```
% Amplifier
V_max = 12;
Theta_max = 2*pi;
% Motor
J_motor = 0.0425; % Motor moment of inertia
L_motor = 1.066e-3; % Motor inductance
R_motor = 0.000044; % Motor coil resistance
C_motor = 0.00025;
K_t = 0.02271; %  Motor torque constant
% Pulleys
r_large = 20;
```

```
r_small = 1;
% Solar panel configuration
J_panels = 778.58256;
C_panels = 0.05;
% Wind parameters
C_m = 0.8; % Drag coefficient
A = 13.13; % Combined area of the panels (m^2)
d = 0.826;
b = 0.944;
rho = 1.225; % Density of the air (kg.m^3)

% Winter or summer
Summer  = 355; % 21 December

winter = 172; % 21 June
```

B.2 Solar position calculator

```
Summer  = 355; % Day out of 365 that has been taken to represent Summer
winter = 172; % Day out of 365 that has been taken to represent Winter
day= summer;
declination_angle=23.45*sin(360*(284+day)/365*pi/180); %see equ(1)
d=declination_angle*pi/180;
h_mor_time = 6; % Time (Sunrise) when the solar tracker is activated
h_even_time = 17; % Time (Sunset) when the solar tracker stops tracking the Sun
for k = h_mor_time:1:h_even_time % Loop that ensures that the Sun's angle is
tracked every minute
    for m = 0:1:59
        h = ((k+m/60)-12)*15*pi/180; % Hour angle calculation by eqn 17 in radians
        B=0*pi/180; % Elevation of the the Sandton area in rad
        L=26*pi/180; % Latitude of the Sandton area
        Z=10*pi/180; %
        Daily_optimum_tilt_angle=(L-d)*180/pi; % Calculation of the daily optimum
tilt angle
        Altitude_angle= asin(sin(L)*sin(d)+cos(L)*cos(d)*cos(h))*180/pi; %
Calculation of the altitude angle
        a=Altitude_angle*pi/180;
        Solar_zenith_angle=90-Altitude_angle; % Calculation of the zenith angle
```

```
        phi=Solar_zenith_angle*pi/180;
        Solar_azimuth_angle= asin(cos(d)*sin(h)/cos(a))*180/pi; % Calculation of
the Solar azimuth angle
        if i < 12
        z=Solar_azimuth_angle*pi/180;
        Incidence_angle= -acos(sin(L)*sin(d)*cos(B)-
cos(L)*sin(d)*sin(B)*cos(Z)+cos(L)*cos(d)*cos(h)*cos(B)+sin(L)*cos(d)*cos(h)*sin(B
)*cos(Z)+cos(d)*sin(h)*sin(B)*sin(Z));%*180/pi;
        theta(i-5,j+1) = Incidence_angle; % Calculation of the angle of incidence
        else
        Incidence_angle= acos(sin(L)*sin(d)*cos(B)-
cos(L)*sin(d)*sin(B)*cos(Z)+cos(L)*cos(d)*cos(h)*cos(B)+sin(L)*cos(d)*cos(h)*sin(B
)*cos(Z)+cos(d)*sin(h)*sin(B)*sin(Z));%*180/pi;
        theta(i-5,j+1) = Incidence_angle; % Calculation of the angle of incidence
        end
        time(k-5,m+1) = [i+(j/60)];
    end
 final_mat = [];
 final_time = [];
 Suns_path = [];
    for w = 1:1:12
        for q = 1:1:60
             ff = theta(w,q);
             tf = time(w,q);
         final_mat = [final_mat;ff];
         final_time = [final_time;tf];
         Suns_path = [final_time final_mat]; % Matrix that stores the Sun's
angular position with time
        end
     end
end
```

Manufacturer components

Solar panel selection catalogue

Figure 0.1: Solar panel catalogue

Motor selection catalogue

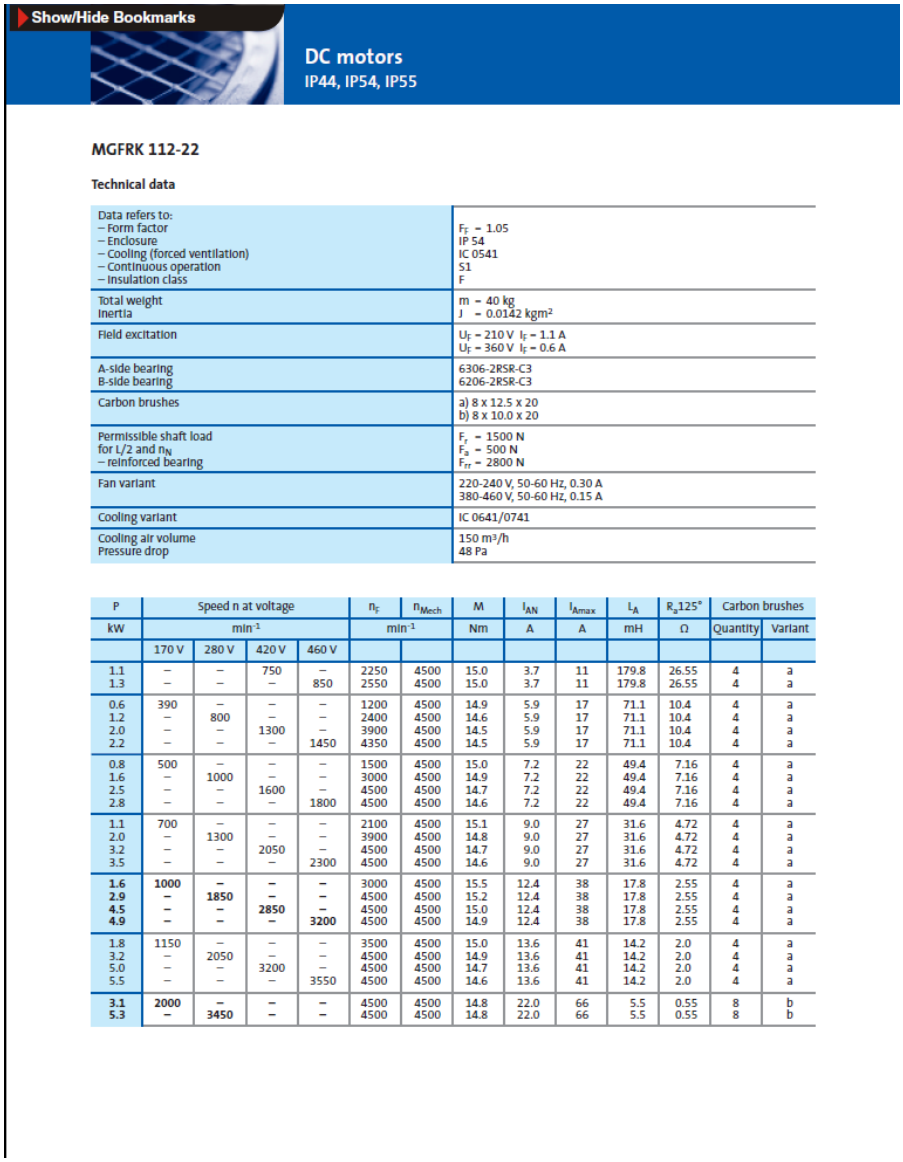

Show/Hide Bookmarks

DC motors
IP44, IP54, IP55

MGFRK 112-22

Technical data

Data refers to: – Form factor – Enclosure – Cooling (forced ventilation) – Continuous operation – Insulation class	F_F = 1.05 IP 54 IC 0541 S1 F
Total weight Inertia	m = 40 kg J = 0.0142 kgm²
Field excitation	U_F = 210 V I_F = 1.1 A U_F = 360 V I_F = 0.6 A
A-side bearing B-side bearing	6306-2RSR-C3 6206-2RSR-C3
Carbon brushes	a) 8 x 12.5 x 20 b) 8 x 10.0 x 20
Permissible shaft load for L/2 and n_N – reinforced bearing	F_r = 1500 N F_a = 500 N F_{rr} = 2800 N
Fan variant	220-240 V, 50-60 Hz, 0.30 A 380-460 V, 50-60 Hz, 0.15 A
Cooling variant	IC 0641/0741
Cooling air volume Pressure drop	150 m³/h 48 Pa

P	Speed n at voltage				n_F	n_{Mech}	M	I_{AN}	I_{Amax}	L_A	R_a125°	Carbon brushes	
kW	min⁻¹				min⁻¹		Nm	A	A	mH	Ω	Quantity	Variant
	170 V	280 V	420 V	460 V									
1.1	–	–	750	–	2250	4500	15.0	3.7	11	179.8	26.55	4	a
1.3	–	–	–	850	2550	4500	15.0	3.7	11	179.8	26.55	4	a
0.6	390	–	–	–	1200	4500	14.9	5.9	17	71.1	10.4	4	a
1.2	–	800	–	–	2400	4500	14.6	5.9	17	71.1	10.4	4	a
2.0	–	–	1300	–	3900	4500	14.5	5.9	17	71.1	10.4	4	a
2.2	–	–	–	1450	4350	4500	14.5	5.9	17	71.1	10.4	4	a
0.8	500	–	–	–	1500	4500	15.0	7.2	22	49.4	7.16	4	a
1.6	–	1000	–	–	3000	4500	14.9	7.2	22	49.4	7.16	4	a
2.5	–	–	1600	–	4500	4500	14.7	7.2	22	49.4	7.16	4	a
2.8	–	–	–	1800	4500	4500	14.6	7.2	22	49.4	7.16	4	a
1.1	700	–	–	–	2100	4500	15.1	9.0	27	31.6	4.72	4	a
2.0	–	1300	–	–	3900	4500	14.8	9.0	27	31.6	4.72	4	a
3.2	–	–	2050	–	4500	4500	14.7	9.0	27	31.6	4.72	4	a
3.5	–	–	–	2300	4500	4500	14.6	9.0	27	31.6	4.72	4	a
1.6	**1000**	**–**	**–**	**–**	3000	4500	15.5	12.4	38	17.8	2.55	4	a
2.9	**–**	**1850**	**–**	**–**	4500	4500	15.2	12.4	38	17.8	2.55	4	a
4.5	**–**	**–**	**2850**	**–**	4500	4500	15.0	12.4	38	17.8	2.55	4	a
4.9	**–**	**–**	**–**	**3200**	4500	4500	14.9	12.4	38	17.8	2.55	4	a
1.8	1150	–	–	–	3500	4500	15.0	13.6	41	14.2	2.0	4	a
3.2	–	2050	–	–	4500	4500	14.9	13.6	41	14.2	2.0	4	a
5.0	–	–	3200	–	4500	4500	14.7	13.6	41	14.2	2.0	4	a
5.5	–	–	–	3550	4500	4500	14.6	13.6	41	14.2	2.0	4	a
3.1	**2000**	**–**	**–**	**–**	4500	4500	14.8	22.0	66	5.5	0.55	8	b
5.3	**–**	**3450**	**–**	**–**	4500	4500	14.8	22.0	66	5.5	0.55	8	b

Figure 0.2: Motor selection catalogue